Bull. Mater. Sci., Vol. 32, No. 5, October 2009, pp. 465–470. © Indian Academy of Sciences.

Preparation and characterization of nano-hydroxyapatite powder using sol–gel technique

K P SANOSH[†], MIN-CHEOL CHU, A BALAKRISHNAN[†], T N KIM[†] and SEONG-JAI CHO*

Division of Metrology for Emerging Technology, Korea Research Institute of Standards and Science, 1 Doryong-Dong, Yuseong-Gu, Daejeon 305-340, Republic of Korea

[†]Department of Information and Electronic Materials Engineering, College of Engineering, Paichai University, Daejeon 302-735, Republic of Korea

MS received 29 August 2008; revised 12 December 2008

Abstract. **Hydroxyapatite (HA) nano powders (20–60 nm) were synthesized using a sol–gel route with calcium nitrate and phosphoric acid as calcium and phosphorus precursors, respectively. Double distilled water was used as a diluting media for HA sol preparation and ammonia was used to adjust the pH. After aging, the HA gel was dried at 65°C and calcined to different temperatures ranging from 200–800°C. The dried and calcined powders were characterized for phase composition using X-ray diffractometry, elemental dispersive X-ray and Fourier transform infra-red spectroscopy. The particle size and morphology were studied using transmission electron microscopy. Calcination revealed HA nano powders of increased particle size and crystallinity with increase in temperature. For all calcinations temperatures, the particle size distribution analysis of HA powders showed skewed distribution plot. At temperature of 700°C and above, formation of CaO was noticed which was attributed to phosphorous volatilization. This study showed that high purity HA with varying degrees of crystallinity could be obtained using this simple technique.**

Keywords. **Hydroxyapatite; particle size; sol–gel; calcination; phase purity; crystallinity.**

1. Introduction

Hydroxyapatite (HA) has attracted much attention as a material for artificial bones (Hench 1998), scaffolds for tissue engineering (Ebaretonbofa and Evans 2002; Li *et al* 2002) and chromatographic packing (Kawasaki 1999) because of its high bioactivity and particular adsorbability for various ions and organic molecules. Due to the chemical similarity between HA and mineralized bone of human tissue, synthetic HA exhibits strong affinity to host hard tissues. Formation of chemical bond with the host tissue offers HA a greater advantage in clinical applications than most other bone substitutes, such as allografts or metallic implants (Itokazu *et al* 1998; Minguez *et al* 1990). However, due to poor mechanical properties of HA the recent trend in bioceramic research is focused on improving their mechanical and biological properties using nanotechnology. It has been reported that the resorption process of HA is quite different from that of bone mineral. Bone mineral crystals are nano-sized with a very large surface area. These crystals are grown in an organic matrix and have very loose crystal to crystal bonds. Therefore, the resorption by osteoclasts is quite homogeneous. On the contrary, micro-size HA presents a low surface area and have strong crystal–to–crystal bond. In addition, the bone mineral shows higher bioactivity compared with crystalline HA (Kim 2003). Moreover, studies on the *in vitro* and *in vivo* Ca^{2+} ion release (Murugan and Ramakrishna 2004) from the nano HA powders were found to be similar to bone apatite and significantly faster than microscale sized counterparts. Thus engineering HA at nano-level would have superior functional properties due to its grain size, large surface area to volume ratio and crystallinity similar to biological apatite, which would have a greater impact on implant-cell interaction in body environment (LeGeros 1991). Hence extensive efforts have been made to produce synthetic nano-HA materials (LeGeros 1991). Common methods used to produce synthetic nanocrystalline HA include precipitation (Saeri *et al* 2003), hydrothermal (Masahiro *et al* 1994), hydrolysis (Shih *et al* 2004), mechanochemical (Silva *et al* 2003) and sol–gel (Kim and Kumta 2004). These techniques can generate nano to micrometric size HA crystals (Dean-Mo *et al* 2001; Afshar *et al* 2003). However, sol–gel (Kim and Kumta 2004) method offers a distinct advantage of a molecular-level mixing of the calcium and phosphorus precursors, which is capable of

*Author for correspondence (the_krecian@yahoo.com)

improving chemical homogeneity of the resulting HA to a significant extent, in comparison with above conventional techniques. Furthermore, the high reactivity of the sol–gel powders results in the decrease of the calcining and sintering temperatures (Dean *et al* 2002). In the present work, the synthesis of a nanosize HA powder via sol–gel method was prepared using calcium nitrate tetrahydrate, phosphoric acid (H_3PO_4) and ammonia as starting precursors. Pure HA nano powders were obtained at 65–600°C.

2. Experimental

In the present study, calcium nitrate tetrahydrate ($Ca(NO_3)_2{\cdot}4H_2O$) (CNT) (Junsei chemicals Co., Ltd., S. Korea), phosphoric acid (H_3PO_4) (PA) (Samchun Pure Chemicals Co., Ltd, S. Korea) and ammonia (NH_3) (Daejung Chemicals and Metals Co. Ltd., S. Korea) were used as starting precursors. The schematic presentation of the procedure is given in figure 1. Firstly, 0·25 M PA was prepared in double distilled water. To this solution, ammonia was added and stirred till a constant pH = 10 was obtained. 1 M CNT was prepared by completely dissolving it in double distilled water. This CNT solution was slowly added to the above PA–ammonia solution, maintaining a Ca/P ratio of 1·67. The solution was kept constant at pH = 10 by further adding small amounts of ammonia. The solution was rigorously stirred for 1 h and kept for ageing for 24 h at room temperature. The gel obtained after aging was dried at 65°C for 24 h in a dry oven. The powders from dried gel were washed repeatedly using double distilled water to remove NH_4^+ and NO_3^-. After washing, the powder was calcined in air at different temperatures ranging from 200–800°C for 30 min using an electrical furnace and employing a heating rate of 10°C/min. Transmission electron microscope (TEM) (HR-TEM, Model Tecnai–Philips F30, FEI Co., Hillsboro) was used to observe the morphology and the particle size of calcined HA powders. Elemental phase composition of the HA powder was analyzed using energy dispersive X-ray (EDX) (SEM-EDX, ISI-DS130C dual stage SEM, Akashi, Japan). The X-ray diffraction (XRD) pattern of the final HA nanoparticles was obtained with CuKα radiation (λ = 1·5418 Å) on a D8 Advance (Bruker-AXS, Germany) diffractometer and then analysed using Ni-filtered CuKα radiation (λ = 0·1542 nm), in the step scanning mode, with tube voltage of 40 kV and tube current of 50 mA. The XRD patterns were recorded in the 2θ range of 20–60°, with a step size of 0·02° and step duration of 0·5 s.

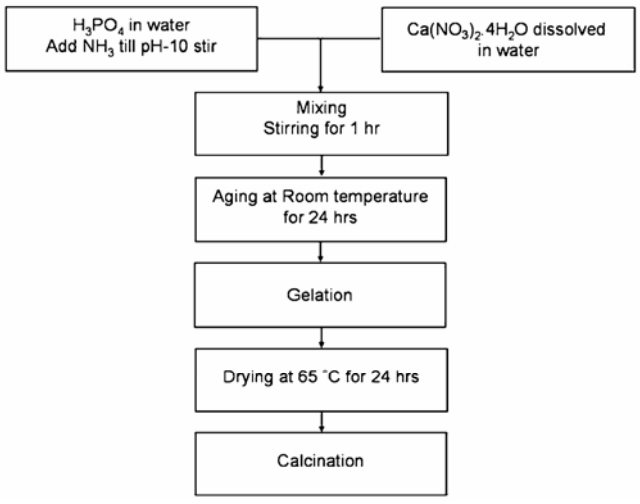

Figure 1. Flow chart of hydroxyapatite preparation by the sol–gel route.

The mean crystallite size (D) of the particles was calculated from the XRD line-broadening measurement from the Scherrer equation (Azaroff 1968):

$$D = \frac{0{\cdot}89\lambda}{\beta\cos\theta}, \tag{1}$$

where λ is the wavelength (CuKα), β the full width at half-maximum of the HA (211) line and θ the diffraction angle.

The fraction of crystalline phase (X_c) of the HA powders was evaluated by the following equation (Landi *et al* 2000)

$$X_c = \frac{1 - V_{112/300}}{I_{300}}, \tag{2}$$

where I_{300} is the intensity of (300) diffraction peak and $V_{112/300}$ the intensity of the hollow between (112) and (300) diffraction peaks of HA.

The particle size distribution of the powder was obtained using a condensation particle counter (GRIMM Aerosol Technik, Gmbh, Germany (serial no 5400)). The Fourier transform infrared spectroscopy (FT–IR) was done with Nexus 6700 FTIR (Thermo-Nicolet, Inc.) equipped with an attenuated total reflectance (ATR) accessory (Smart Miracle, PIKE Tech.).

3. Results and discussion

The reactions involved in the formation of HA during the sol–gel preparation and drying can be expressed as follows

$$H_3PO_4 + 3NH_4OH \rightarrow (NH_4)_3PO_4 + 3H_2O, \tag{i}$$

$$6(NH_4)_3PO_4 + 10Ca(NO_3)_2{\cdot}4H_2O \rightarrow Ca_{10}(PO_4)_6(OH)_2 + 20NH_4NO_3. \tag{ii}$$

The formation of $20NH_4NO_3$ (ammonium nitrate) byproduct was removed by repeated washing with double distilled water.

Figure 2a shows the XRD pattern of HA from 200–800°C. The determined amounts of crystallinity and cry-

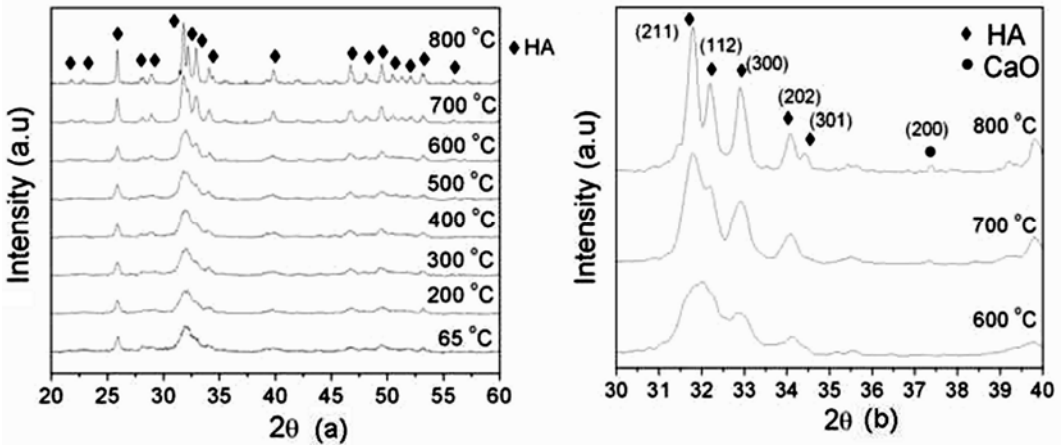

Figure 2. XRD patterns of HA powders (**a**) calcined at different temperatures and (**b**) showing presence of minor CaO phase at 700 and 800°C.

Table 1. Table showing the crystallinity of HA and comparing the particle size obtained from XRD and PSD at different calcination temperatures.

Calcination temperature (°C)	Crystallinity (%)	Crystallite size, D (nm)	PSD* (nm)
65	6 ± 1·1	18 ± 1·5	20
200	12 ± 2·5	24 ± 1·3	32
300	33 ± 2·2	28 ± 2·0	–
400	44 ± 3·5	31 ± 1·9	37
500	57 ± 2·7	28 ± 2·8	–
600	64 ± 3·4	39 ± 2·2	45
700	78 ± 4·0	54 ± 3·1	–
800	88 ± 2·5	61 ± 1·5	58

*Particle size value obtained from centre of skewed distribution curve in figure 4.

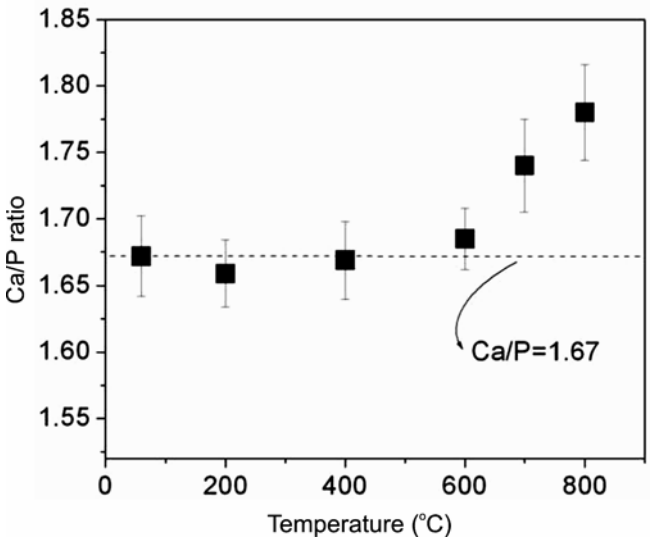

Figure 3. Plot of variation of Ca/P with calcination temperature.

stallite size (determined by Scherrer equation) from XRD of five calcined HA samples for each temperature are given in table 1. It could be observed that the increase in HA crystallinity with the increase in calcination temperature is not linear. Similar phenomenon was observed by Bouyer *et al* (2000). It was also reported that HA calcined at higher temperatures exhibiting good crystallinity, shows little or no activity towards bioresorption, which is important for the formation of chemical bonding with surrounding hard tissues (Aoki 1994; Currey 2001). Thus the amorphous HA powders that were obtained at lower temperatures in this study are expected to be more metabolically active than the fully developed crystalline hydroxyapatite structure which otherwise is nonsoluble in physiological environment (Kim *et al* 2000). XRD patterns of the dried HA gel powder calcined at temperatures 600°C and below showed mainly broad peaks of HA and no characteristic peaks of impurities were observed, indicating that the product was of high purity. Heating HA powder at 700°C and above induced a high crystalline HA diffraction peaks together with minor CaO peaks (figure 2b). The volume fraction of CaO (V_{CaO}) was calculated using the following equation (Balakrishnan *et al* 2007)

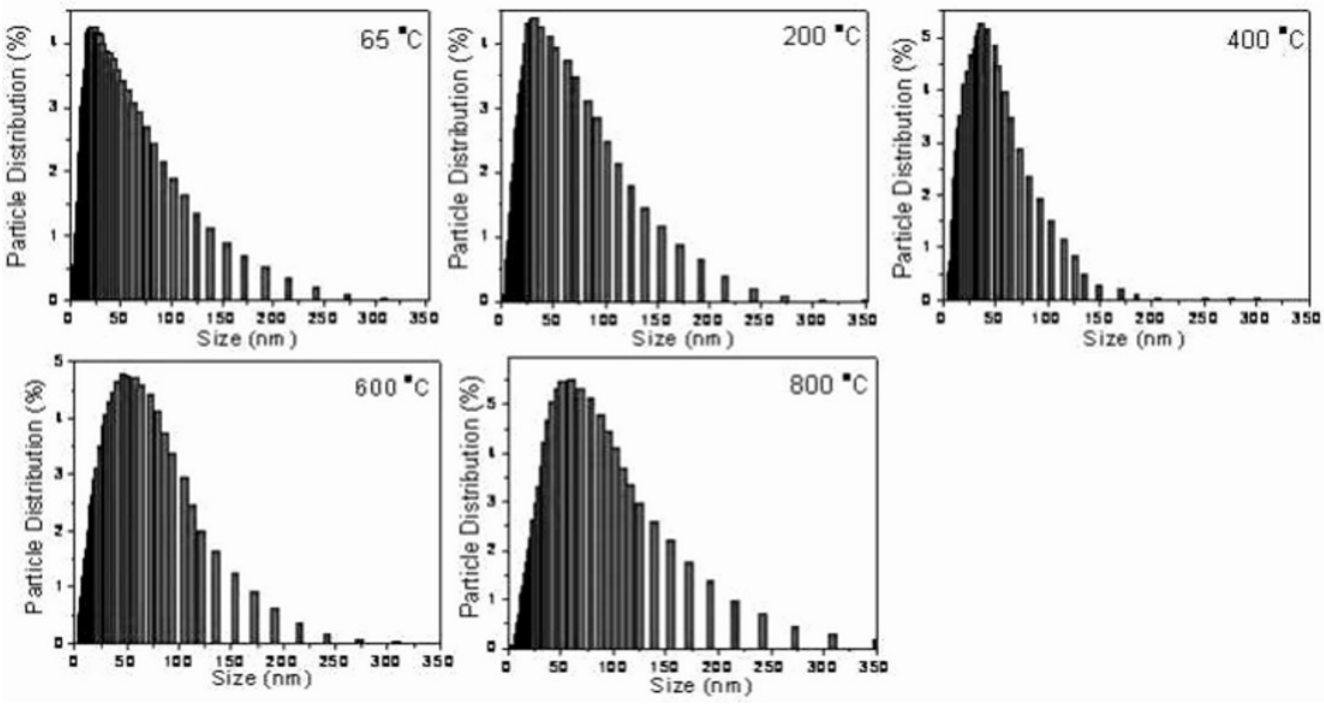

Figure 4. Plot showing the variation in particle size distribution with the change in calcination temperature.

$$V_{CaO} = \frac{I_{CaO_1} + I_{CaO_2}}{I_{CaO_1} + I_{CaO_2} + I_{HA}}, \quad (3)$$

where I_{CaO_1} and I_{CaO_2} are the intensities of the two strongest peaks of CaO phase, I_{HA} the intensity of strongest peak of HA phase. The small amount of CaO at 700 and 800°C was found to be ~0·5 ± 0·2 and 2 ± 0·5%, respectively. (Note: Because of the very low intensity of CaO peaks, $I_{CaO_2} = 0$ was taken).

The Ca/P stoichiometry of calcined HA at different temperatures (five samples each) (figure 3) was analysed using EDX. Analysing figures 2b and 3, it can be seen that HA powder with a Ca/P ratio near to 1·67 i.e. at temperature 600°C and below, showed no CaO contents and that with a Ca/P ratio near to 1·75 and above, showed the formation of minor amounts of CaO i.e. for calcined samples at 700°C and above. Other researchers have also reported similar formation of CaO in sol–gel processing of HA (Lopatin *et al* 1998; Varma *et al* 1998). Studies by Chai and Ben-Nissan (1999) indicate that phosphorus-containing precursors have high potential for volatilization above 650°C (Szu *et al* 1992), hence $Ca(NO_3)_2$ molecules may not get completely incorporated into the complex which is evident by higher Ca/P molar ratio (figures 2b and 3) at 700°C and above.

The particle size distribution (PSD) plot (figure 4) showed a skewed distribution which centred to larger particle size with the increase in temperature. The PSD value centred for each temperature was found to be in proximity with the (table 1) crystallite size obtained from the Scherrer equation. Figure 5(a and b) shows the TEM image of the HA calcined at 600°C for 30 min with prolate spheroidal phase structure (figure 5b). Certain agglomeration (figure 5a) of HA particles was observed. The nucleation and growth of HA with temperature can be described by nucleation–aggregation–agglomeration-growth mechanism theory explained earlier (Randolph and Larson 1986; Rodríguez *et al* 1998). According to this mechanism, HA particle goes through following steps: (a) nucleation and growth to form HA nanocrystallites, (b) aggregation of elemental nanocrystals by molecular attractions (Gomez *et al* 2001) of different nanometric/colloidal scale forces which cause surface free energy minimization, (c) further crystal growth, at a constant residual supersaturation, acting as cementing agent inside the aggregates to form agglomerate. The increase in particle size with temperature takes place by aggregation of these agglomerated particles to form secondary particle. This has been schematically represented in figure 6.

FT–IR patterns presented in figure 7 confirm the formation of HA calcined at 600°C. The spectra possessed a very weak band at 3720 cm^{-1}, sharp and strong band at 3572 cm^{-1} and a weak broad band ranging between 3550 and 3350 cm^{-1}. The 3720 and 3572 cm^{-1} bands correspond to OH^- group, and the broad band at 3550–3350 cm^{-1}, to strongly adsorbed and/or bound H_2O (Elliot 1994). H_2O band was also observed at 1650 cm^{-1}. A strong band of PO_4^{3-} group was also seen at 1037 and 967 cm^{-1}. The bands obtained for respective phosphate

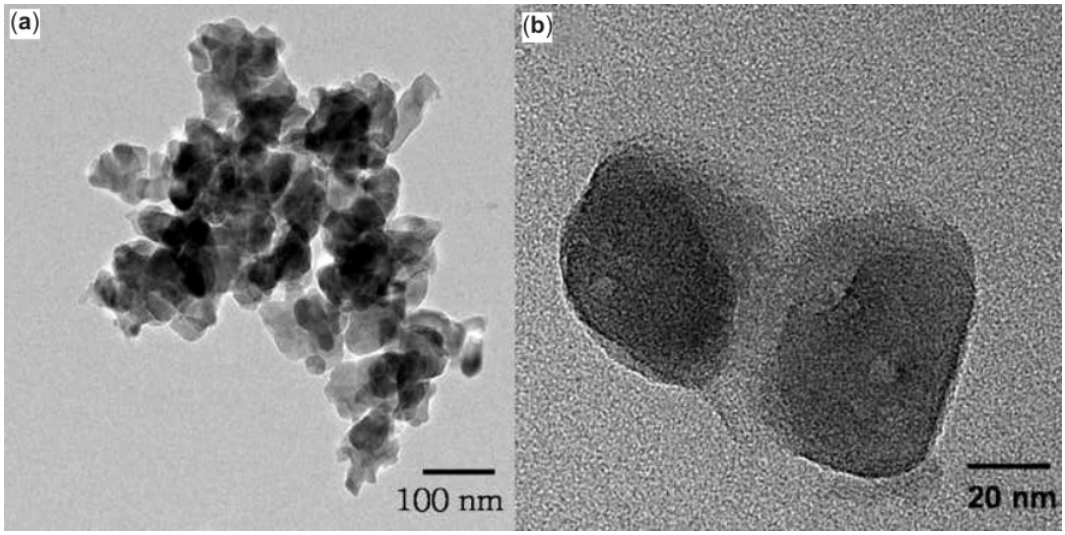

Figure 5. TEM image of calcined HA powders at 600°C showing (**a**) certain agglomeration and (**b**) morphology and size.

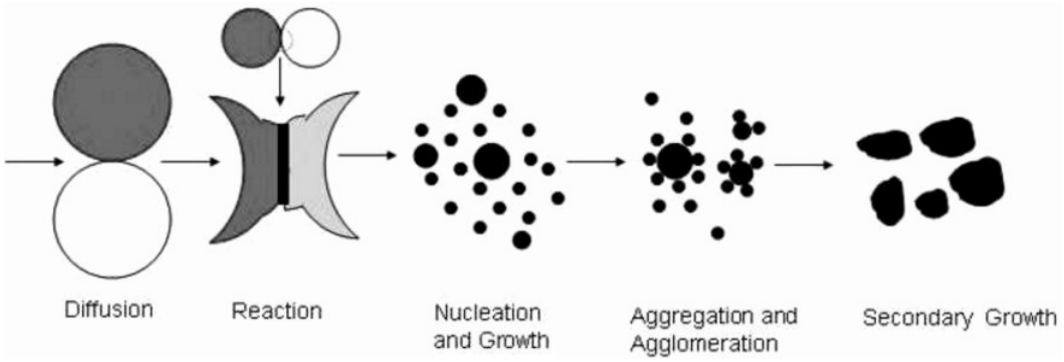

Figure 6. Schematic representation of nucleation and growth of HA (Randolph and Larson 1986; Rodríguez *et al* 1998).

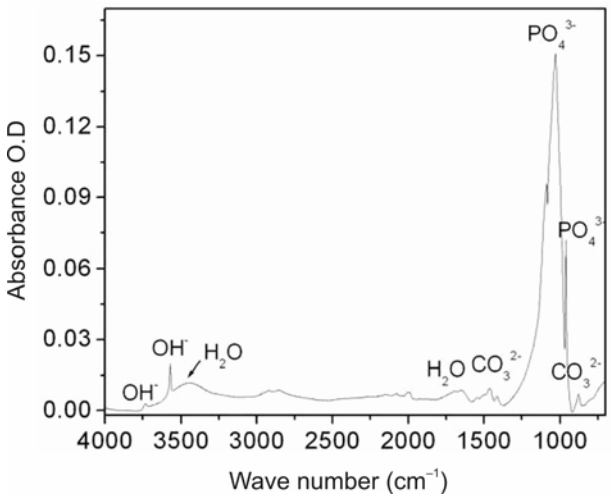

Figure 7. FT–IR patterns showing the formation of HA calcined at 600°C.

and hydroxyl groups of pure HA, were in agreement with other published data (Montel *et al* 1980; Rehman and Bonfield 1997). A weak band of CO_3^{2-} was detected in the region around 1465 and 875 cm^{-1}. The band at 875 cm^{-1} indicates *n*2 mode of CO_3^{2-} group (Elliott 1994; Emerson and Fischer 1962) and it suggests a minor amount of B-type carbonate substitution i.e. small part of the PO_4 (B-type) groups in the apatitic structure was replaced by CO_3. The characteristic bands from inorganic carbonate ion suggest that carbon gets dissolved in the organics from atmosphere and does not pyrolyze completely and may instead dissolve into the HA crystal. Since carbonates are constituents of bone structures (Rajabi-Zamani *et al* 2008), the presence of CO_3 may improve the bioactivity of HA rather than being a cause of concern.

4. Conclusions

In this study, the synthesis of a nanostructured hydroxyapatite powder via sol–gel method is reported using calcium and phosphorous precursors. This process showed that high purity product of nano-HA powders could be

obtained at low temperatures. The crystallinity, particle size and Ca/P ratio of the resulting nanoparticles were found to be dependent on the calcination temperature. When Ca/P ratio exceeded 1·75, formation of CaO phase was observed, which was attributed to phosphorous volatilization. FTIR results showed dissolution of small amount of CO_3^{2-} into the HA crystal, possibly due to dissolution of CO_2 from atmosphere during calcinations at 600°C. The method of synthesis showed that the biocompatible nanocrystals (20–60 nm) of HA, with varying degree of crystallinity, can be effectively synthesized using this simple technique.

References

Afshar A, Ghorbani M, Ehsani N, Saeri M R and Sorrell C C 2003 *Mater. Des.* **24** 197

Aoki H 1994 *Medical applications of hydroxyapatite* (Tokyo: Ishiyaku EuroAmerica)

Azaroff L A 1968 *Elements of X-ray crystallography* (New York: McGraw-Hill)

Balakrishnan A, Panigrahi B B, Chu M C, Yoon K J, Kim T N and Cho S J 2007 *J. Mater. Res.* **22** 2550

Bouyer E, Gitzhofer F and Boulos M I 2000 *J. Mater. Sci. Mater. Med.* **11** 523

Chai C S and Ben-Nissan B 1999 *J. Mater. Sci. Mater. Med.* **10** 465

Currey J 2001 *Nature* **414** 699

Dean-Mo L, Troczynski T and Tseng W J 2001 *Biomaterials* **22** 1721

Dean-Mo L, Quanzu Y, Tom T and Wenjea J T 2002 *Biomaterials* **23** 1679

Ebaretonbofa E and Evans J G 2002 *J. Porous Mater.* **9** 257

Elliott J C 1994 *Structure and chemistry of the apatites and other calcium orthophosphates* (Amsterdam: Elsevier)

Emerson W H and Fischer E E 1962 *Arch. Oral Biol.* **7** 671

Gomez-Morales J, Torrent-Burgues J and Rodriguez-Clemente R 2001 *Cryst. Res. Technol.* **36** 1065

Hench L L 1998 *J. Am. Ceram. Soc.* **81** 1705

Itokazu M, Yang W, Aoki T and Kato N 1998 *Biomaterials* **19** 817

Kawasaki T 1999 *J. Chromatogr.* **544** 147

Kim H M 2003 *J. Curr. Opin. Solid State Mater. Sci.* **7** 289

Kim H M, Kim Y, Park S J, Rey C, Lee H M, Gimcher M J and Ko J S 2000 *Biomaterials* **21** 1129

Kim I S and Kumta P N 2004 *Mater. Sci. Eng.* **B111** 232

Landi E, Tampieri A, Celotti G and Sprio S 2000 *J. Eur. Ceram. Soc.* **20** 2377

LeGeros R Z 1991 *Calcium phosphates in oral biology and medicine* (Basel: H.M. Myers) p. 154

Li S H, De Wijn J R, Layrolle P and de Groot K J 2002 *Biomed. Mater. Res.* **1** 109

Lopatin C M, Pizziconi V, Alford T L and Laursen T 1998 *Thin Solid Films* **326** 227

Masahiro Y, Hiroyuki S, Kengo O and Koji I 1994 *J. Mater. Sci.* **29** 3399

Minguez F, Agra M, Luruena S, Ramos C and Prieto J 1990 *Drugs Exp. Clin. Res.* **16** 231

Montel G, Bonel G, Trombe J C, Heughebaert J C and Rey C 1980 *Pure Appl. Chem.* **52** 973

Murugan R and Ramakrishna S 2004 *Biomaterials* **25** 3073

Rajabi-Zamani A H, Behnamghader A and Kazemzadeh A 2008 *Mater. Sci. Eng.* **C28** 1326

Randolph A D and Larson M A 1986 *Theory of particulate processes* (New York: Academic Press) 2nd edn

Rehman I and Bonfield W 1997 *J. Mater. Sci., Mater. Med.* **8** 1

Rodríguez-Clemente R, López-Macipe A, Gómez-Morales J, Torrent-Burgués J and Castãno V M 1998 *J. Eur. Ceram. Soc.* **18** 1351

Saeri M R, Afshar A, Ghorbani M, Ehsani N and Sorrell C C 2003 *Mater. Lett.* **57** 4064

Shih W J, Yung-Feng C, Moo-Chin W and Min-Hsiung H 2004 *J. Cryst. Growth* **270** 211

Silva C C, Pinheiro A G, Miranda M A R, Góes J C and Sombra A S B 2003 *Solid State Sci.* **5** 553

Szu S P, Klein L C and Greenblatt M 1992 *J. Non-Cryst. Solids* **143** 21

Varma H K, Kalkura S N and Sivakumar R 1998 *Ceram. Int.* **24** 467